JOURNAL OF AIRCRAFT
Vol. 43, No. 3, May–June 2006

Numerical Investigation of Low-Aspect-Ratio Wings at Low Reynolds Numbers

P. Cosyn* and J. Vierendeels†
Ghent University, 9000 Ghent, Belgium

A numerical analysis is performed to study the flow around low-aspect-ratio (LAR) wings and more particularly the resulting lift-and-drag force. The research is focused on low-Reynolds-number aerodynamics, as LAR wings are crucial for the development of microair vehicles (MAVs). The flow around LAR wings is characterized by complex three-dimensional flow phenomena. These phenomena include wing-tip vortices, flow separation and reattachment, laminar to turbulent transition, and a mutual interaction among these phenomena. The flow is studied using a commercial computational fluid dynamics (CFD) program and a strip method. The CFD code is used to investigate the three-dimensional flow aerodynamics of rectangular LAR wings with an aspect ratio between 0.5 and 2 at a Reynolds number of 1×10^5. Simulations on a flat plate and a reflex-type low-Reynolds-number profile (S5010), which is representative for a flying-wing MAV, are performed and compared. Experimental data is used for comparison and validation. The effects of flow separation and low Reynolds numbers are further investigated using a strip method. Two accurate formalized methods to predict lift and drag are derived. The first method is applicable to profiled wings with moderate low-Reynolds-number effects. The second method, which is based on the strip method, is more general and is also applicable to flat plates and wings exhibiting large regions of flow separation.

Nomenclature

AR	=	aspect ratio of the wing, which is the ratio of the total wing span and the chord
C_D	=	total drag coefficient
$C_{D,0}$	=	drag coefficient at zero lift
$C_{D,v}$	=	vortex drag coefficient
C_L	=	total lift coefficient
$C_{L,p}$	=	potential (or linear) lift coefficient
$C_{L,v}$	=	vortex lift coefficient
$C_{L,\alpha}$	=	lift-curve slope (1/deg)
$C_{N,v}$	=	normal force coefficient of the tip vortex suction
D	=	drag force of a strip
d	=	drag force corresponding to the effective angle of attack of a strip
e	=	Oswald factor (or efficiency factor)
K	=	induced drag factor
K_p	=	potential (or linear) lift parameter
$K_{v,le}$	=	vortex lift parameter of the leading edge
$K_{v,se}$	=	vortex lift parameter of the side edges
K_v	=	vortex lift parameter of leading and side edges
L	=	lift force of a strip
l	=	lift force corresponding to the effective angle of attack of a strip
Re	=	Reynolds number based on the chord length and freestream velocity
Re_{2D}	=	Reynolds number based on the chord length and local velocity of a strip
V_∞	=	freestream velocity
V_{2D}	=	local velocity (corresponding to the effective angle of attack of a strip)
α	=	angle of attack
α_{2D}	=	effective angle of attack
ε	=	downwash angle

Received 8 April 2005; presented as Paper 2005-4609 at the AIAA 23rd Applied Aerodynamics Conference, Toronto, ON, Canada, 6–9 June 2005; revision received 19 September 2005; accepted for publication 19 September 2005.

*Ph.D. Student, Department of Flow, Heat and Combustion Mechanics, St. Pietersnieuwstraat 41. Member AIAA.

†Professor, Department of Flow, Heat and Combustion Mechanics, St. Pietersnieuwstraat 41. Member AIAA.

I. Introduction

SMALL unmanned aerial vehicles and microair vehicles (MAVs) are at the forefront of the current aeronautical research. They were first defined by DARPA (Defense Advanced Research Projects Agency) as six degree-of-freedom robots able to perform a variety of missions, including reconnaissance, surveillance, targeting, and biochemical sensing.[1] A maximum dimension of 15 cm (6 in.) and a payload mass of 18 g (0.63 oz) was imposed as a first goal but, depending on the missions and payloads, slightly larger MAVs need to be developed. The MAVs may include sensors, an autopilot, a global positioning system navigation, and other equipment. The technological advancements in microelectronics and MEMs (microelectromechanical systems), which make it possible to construct such vehicles, and the multitude of interesting applications play a big role in the development of this new class of flight vehicle. The research is not limited to fixed-wing MAVs[2–5]; flapping-[6,7] and rotating-wing[8] MAVs are also being developed for indoor missions.

However, the design of fixed-wing MAVs is hindered by a lack of accurate models that can predict the primary aerodynamic forces necessary for performance and dynamics-related optimization studies. Classical aerodynamic theory, which is an accurate predictive tool for the development of large-scale aircraft, is generally not applicable for LAR wings at low Reynolds numbers. The reason is twofold. Classical aerodynamic theory is limited to turbulent (high-Reynolds-number) flows, and these do not exhibit complex flow phenomena such as laminar separation bubbles. Those bubbles are difficult to control and have generally a negative drawback on drag. A second reason is the limited research and aerodynamic models that exist on LAR wings. Theories on LAR wings exist, but they are focused on delta planforms for transonic or supersonic airplanes. Nevertheless, there are some useful theories on LAR wings originally developed for wings at higher Reynolds numbers,[9–11] and there are also important experimental results available on LAR flat plates at low Reynolds numbers.[12,13] Both are used in this research to validate the numerical results and to find appropriate equations for lift and drag.

Before investigating the numerical results, it is useful to have a clear picture in mind of the flow around a LAR wing. Figure 1 gives

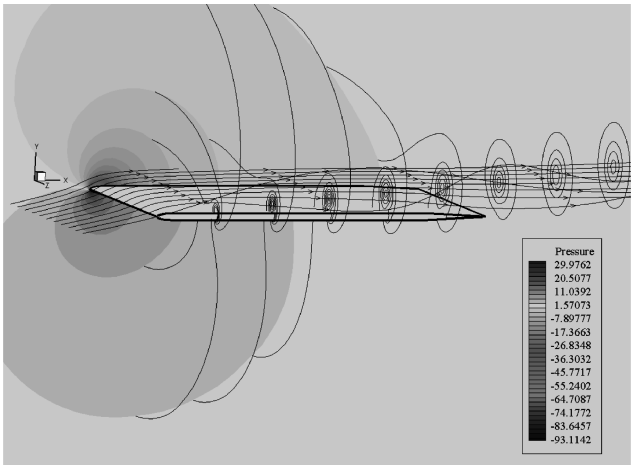

Fig. 1 Streamtraces and pressure contours of the flow around a flat plate.

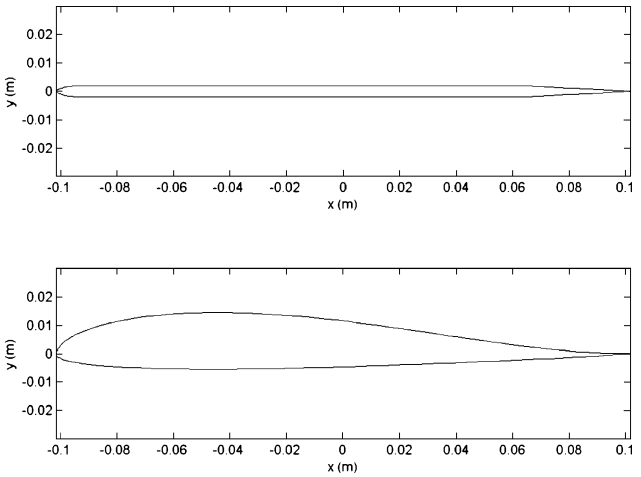

Fig. 2 Flat plate and S5010 geometry.

an idea of the flow around a rectangular surface. Early experimental research indicated that the flow around wings with small aspect ratios could be described by a bound vortex flow and a wing-tip flow characterized by two tip vortices at the side edges of the wing and located above the suction side of the wing.[14] The flow associated with the circulation around the wing is called the "bound vortex flow." This is the flow that can be found using lifting-surface theories or inviscid numerical methods such as vortex lattice methods. The bound vortex generates a downwash and sidewash distribution along the wing. The former influences the linear lift and is responsible for the associated induced drag, and the latter leads to the formation of a shear layer at the side edges. The flow around a wing is viscous but the viscous effects can be reduced to a boundary layer at the surface that is responsible for friction drag. If separation (and eventually reattachment) exists, a part of the boundary layer is detached. If those effects are large in extent, they can affect the bound vortex flow and influence the linear lift. This happens when stall occurs, for example. In a low-Reynolds-number flow, the flow around an airfoil is more susceptible to boundary-layer detachment because the flow remains laminar for a significant part of the chord length. A secondary effect of the bound vortex flow is the formation of the shear layer at the side edges. The shear layer is responsible for the tip vortices. The free shear layer is unstable, starts to roll up, and is stabilized by the axial flow of the freestream. The balance between surface vorticity flux and vorticity transport in the freestream dictates the vorticity accumulation or depletion.[15] The vortices cover a part of the upper surface at the edges and give rise to low-pressure regions. This results in a normal force component on the upper surface of the wing that leads to a nonlinear lift-and-drag component, called vortex lift and vortex drag. Throughout the work the terms *vortex lift* and *vortex drag* refer respectively to the lift and drag generated by the suction effect of the tip vortices on the wing. Tip vortices can be simulated using time-dependent nonlinear vortex panel methods or CFD codes. The present research uses a CFD code.

Concerning low-Reynolds-number behavior, it is known that laminar separation bubbles or laminar separation stall are far less a problem at small-aspect-ratio wings (below two) than at large-aspect-ratio wings (or two-dimensional profiles). It seems that lift and drag are dominated by the tip vortices. Combining a low-aspect-ratio wing with a low-Reynolds-number airfoil may eliminate bubble drag and flow separation up to large C_L values at the interesting Reynolds number range for MAVs (which is approximately between 5×10^4 and 2×10^5).

The numerical investigation is focused on two different types of airfoils with aspect ratios equal to 0.5, 1, 1.5, and 2 and angles of attack ranging between 0 and 20 deg. The first type is a flat plate with a thickness-to-chord ratio of 1.96%, a 5-to-1 elliptical leading edge, and a sharp trailing edge. The geometry is the same as the flat plates used in the experiments of Mueller[12] and Torres and Mueller[13] aside from the fact that Torres and Mueller[13] used an elliptical trailing edge for their LAR flat plates. No noticeable difference in lift and drag was found between a CFD simulation of a flat plate using an elliptical trailing edge and a simulation of a flat plate using a sharp trailing edge. However, the latter simulation converged somewhat faster. The second type is a S5010, which is a low-Reynolds-number airfoil with a reflexed camber line. This airfoil is representative for a flying-wing MAV. Figure 2 shows both profiles. The side edges of the wing are cut off. Therefore, the separation point of the shear layer, which is responsible for the tip vortices, is geometrically defined. From experiments on delta wings, it has been demonstrated that tip vortices are independent from the Reynolds number as long as the separation point of the leading edge vortices are geometrically defined.[16,17]

II. CFD Simulation and Results

A. Fluid Solver

Fluent version 6.1 is used for the simulations. The coupled solver is used with an implicit formulation and a second-order upwind scheme for the flow variables. The Courant number is set to 5. The ideal gas law is chosen for the density, and the Spalart–Allmaras[18] model is used as turbulence model. The choice of this turbulence model is based on two-dimensional simulations and is discussed later. No transition model is implemented in Fluent because of the lack of a well-documented and validated three-dimensional transition model for airfoils at this moment. Low-Reynolds-number effects are addressed indirectly by comparison with experimental results and the use of a strip method. This seems to be beneficial because the different lift and drag components can be analyzed separately.

B. Methodology

The methodology is shown in Fig. 3. First, three-dimensional grids are generated for the S5010 and the flat plate, both with an aspect ratio of one. Next the grid dependency of the three-dimensional grids is checked using three different grid sizes, consisting of 3.7×10^5, 1×10^6, and 2.7×10^6 cells. From this study, basic grids ($AR = 1$) for the S5010 and the flat plate are chosen. The grids for the S5010 and the flat plate with other aspect ratios are obtained by scaling the basic grids. Before the three-dimensional simulations are performed, a series of two-dimensional tests of the flat plate and the S5010 profile are done. Experimental data is available for comparison.[12,13] These simulations are necessary to address a few important questions, such as which turbulence model should be used to predict the lift of the profile accurately and the drag as best as possible? Is the angle of attack at which separation occurs on the flat plate well predicted? Finally, a total of 88 three-dimensional computations are executed on eight different grids for 11 angles of attack. Every computation consists of 1500 iterations. Convergence is normally reached after about 1000 computations. The total computation time of one computation is 26 h on a Compaq Alpha ES45 with 16 Gb of RAM.

C. Grid and Boundary Conditions

The geometries and the grids are generated with Gambit (version 1.3), a preprocessor of Fluent. Because of the symmetry, only half of the wing is simulated. The domain of the flat plate is cylindrical with a radius of 10 times the chord length of the wing and a height of 10 times the span. The chord of the wing is 8 in. (20.32 cm). The domain of the S5010 has a C-shape in order to get a smooth grid. A symmetry condition is imposed at the boundary that is connected to the wing, and a far-field boundary condition is set at the boundaries of the remaining domain. The conditions of the far-field flow are pressure, 10,1325 pa; Reynolds number, 100,000; temperature, 300 K; and turbulence intensity, 0.07%. The direction of the flow is specified in Cartesian coordinates and depends on the angle of attack. The Mach number is derived from the Reynolds number, which is 1×10^5 based on the wing chord. The turbulence intensity of the flow corresponds to the turbulent conditions of the experimental test.[13]

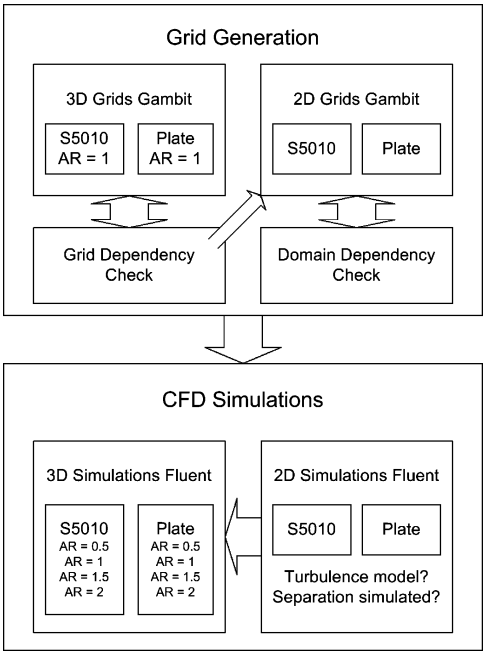

Fig. 3 Methodology.

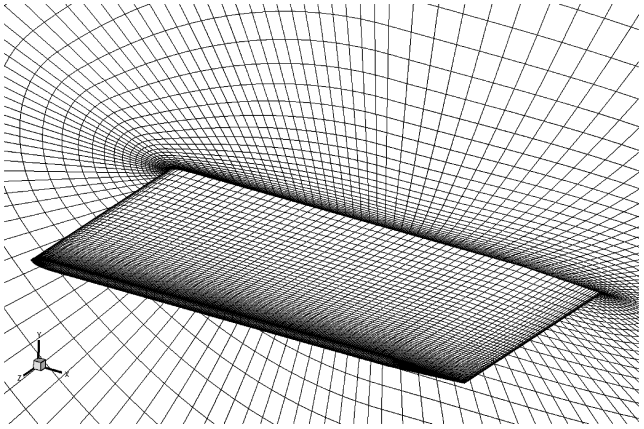

Fig. 4 Flat plate grid, AR = 1.

The grids are composed of unstructured hexahedral cells. The computational domain has a fine grid at the wing and coarsens toward the outer boundary. The grid of the wing surface is refined at the edges (leading edge and side edge) where the largest pressure gradients, due to leading-edge suction and tip vortex, are expected. Figure 4 gives an idea of the grid around a flat plate with 1×10^6 cells.

A grid dependency study shows that 1×10^6 cells are sufficient for an accurate prediction of the lift and drag. A coarse grid with 3.7×10^5 cells performs also reasonably well although it overpredicts the skin friction forces by 7–10%. Because the drag is dominated by pressure drag, this is acceptable. However, because a fine resolution of the wing-tip vortices was desirable, the medium grid with 1×10^6 cells was chosen.

D. Numerical Results

1. Two-Dimensional Simulations

The grid of the two-dimensional simulations is actually the grid of the plane of symmetry of the corresponding three-dimensional grids of the flat plate or S5010. The density of the grid is the same, as well as the boundary conditions and solver settings. This is essential because it represents the ability of the three-dimensional grid to simulate linear lift and profile drag, which is viscous drag and pressure drag of the profile. However, two-dimensional simulations normally require a larger domain to suppress the effect of circulation around the airfoil on the far-field boundary condition. Therefore additional tests were performed with a domain that has a radius five times larger. No significant differences on the lift and drag were found.

The two-dimensional simulations of the S5010 were used to select the best turbulence model. At a Reynolds number of 100,000, experiments on the S5010 show some bubble drag at small angles of attack, but the S5010 has a reasonable constant and low drag level up to 10 deg. From early simulations it was found that the implemented two-equation models of Fluent (k-epsilon and k-omega) had difficulties predicting the drag level at those small Reynolds numbers. The lift was reasonable reproduced, but the profile drag was overpredicted. Many turbulence models were tested, including the k-epsilon realizable, k-epsilon RNG, and k-omega SST models, but the best turbulence model is the Spalart–Allmaras model,[18] which is a one-equation model. Figure 5 illustrates this fact. The k-epsilon realizable model gives more overprediction of the drag, and the k-omega model predicts the stall too early. The Spalart–Allmaras model is a relatively simple one-equation model that solves a modeled transport equation for the kinematic eddy (turbulent) viscosity. This embodies a relatively new class of one-equation models in which it is not necessary to calculate a length scale related to the local shear-layer thickness. The Spalart–Allmaras model was designed specifically for aerospace applications involving wall-bounded flows and gives good results for boundary layers subjected to adverse pressure gradients. Also, the Spalart–Allmaras model is a low-Reynolds-number model, requiring the viscous-affected region of the boundary layer to be properly resolved, which is of course a necessity for wing simulations. From that perspective, it is not surprising that the Spalart–Allmaras model is the best turbulence model. Figure 5 shows also a

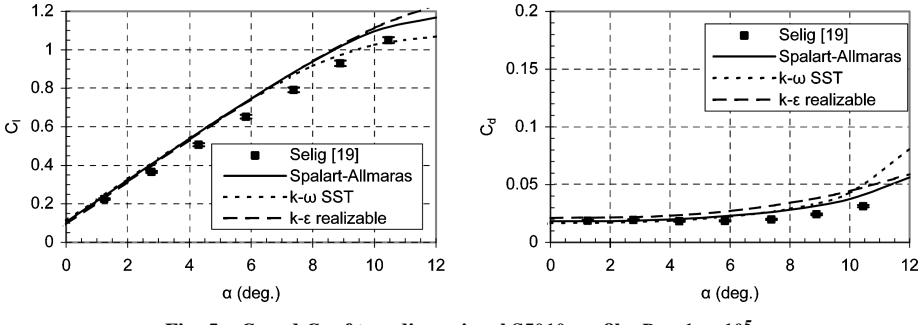

Fig. 5 C_l and C_d of two-dimensional S5010 profile, $Re = 1 \times 10^5$.

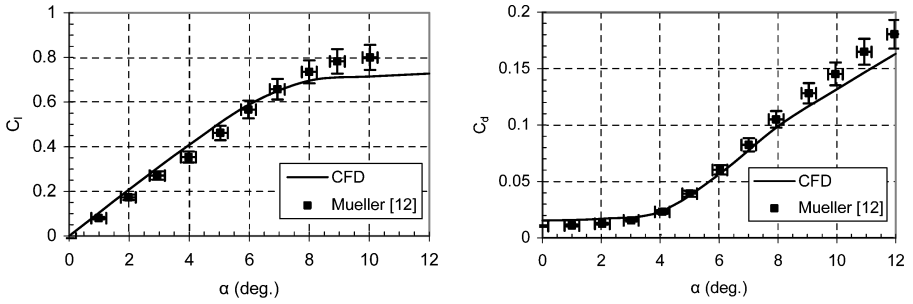

Fig. 6 C_l and C_d of two-dimensional flat plate, $Re = 1 \times 10^5$.

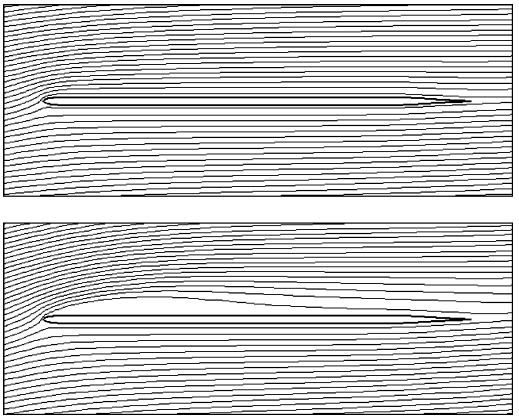

Fig. 7 Streamlines of two-dimensional flat plate (top: $\alpha = 4$ deg, bottom: $\alpha = 6$ deg).

comparison of the two-dimensional simulation of the S5010 with the Spalart–Allmaras model (solid line) and experimental results from Selig.[19] The uncertainty on the experimental data is 1.5% for the lift coefficient and 3% for the drag coefficient. The Reynolds number of the experimental test is 99,700. As expected, the bubble drag is not simulated because a transition model is not implemented. The transition from laminar to turbulent flow happens immediately at the leading edge. Overprediction of the drag in the high alpha range is about 20%, but the absolute value of the difference is less than 0.01, which is negligible compared with three-dimensional drag. This difference is acceptable because the small amount of profile drag does not contribute significantly to the drag of a LAR wing at these angles of attack, unless large regions of separated flow would exist. At high angles of attack the drag of a LAR wing is dominated by the induced drag and vortex drag. Besides the difference in drag, an overprediction of the lift up to 10% is found at high angles of attack. All turbulence models showed an overprediction of the lift. Selig[19] also discussed the overprediction of lift of the numerical computations and attributed it partly to inaccuracy of wind-tunnel data. A second explanation may be the influence of a separation bubble that affects the suction peak at the leading edge and reduces the lift.

The lift and drag of a two-dimensional flat plate is compared to the experimental data of Mueller[12] (Fig. 6). The uncertainty on the experimental data is 7% for the lift-and-drag coefficient and 0.5 deg for the angle of attack. An important feature of the flow is the separation and reattachment that occurs at an angle of attack of about 4–5 deg. The separation is geometrically triggered at the leading edge. The separation results in a kink in the drag coefficients at $\alpha = 4$ deg. The drag is generally well predicted. Only at $\alpha > 8$ deg do the numerical simulations seem to underpredict the drag. In this region, the flow is completely detached and the maximum lift is reached. This regime seems to occur later in the experiments, which explains the higher maximum lift and the higher drag. Experimental results of Mueller[12] indicate that turbulence intensity might have an impact on the lift and drag but only in the stall region. It is in this region that the simple turbulence model has its limitations. This is discussed in Sec. III.A. Figure 7 shows an attached flow condition at 4 deg and a detached flow with reattachment at 6 deg. Reattachment occurs at approximately 50% of the chord.

2. Three-Dimensional Flat-Plate Simulations

The lift and drag of the flat plate is extracted from the numerical data by integrating the pressure and shear stress along the upper surface, lower surface, and the side edge. Figure 8 shows a comparison of C_L and C_D with experimental data.[13] The uncertainty on the experimental data is 5% for the lift-and-drag coefficient and 0.5 deg for the angle of attack. At aspect ratios of 1.5 and 2, the simulation results for the full range are not presented because of vortex shedding (of the bound vortex) at high angles of attack. A steady-state solution could not be found for these situations. The behavior of the lift and drag and the differences between the experimental and numerical data are explained and illustrated later.

AR = 0.5

The flow is dominated by two tip vortices. The lift is well predicted. The drag is slightly underpredicted at high angles of attack. This is a result of the separation and reattachment of the central flow zone. This phenomenon starts at an angle between 12 and 14 deg. This is visible on Fig. 9, which shows the wall shear stress in the X-direction along the top surface for an angle of 14 deg. Negatives values of the wall shear stress in the X-direction indicate the existence of separated flow. The plots show clearly a separated region at the forward central part of the wing. As expected from the two-dimensional simulations, the drag is underpredicted in this region.

AR = 1

This is a mixed-flow condition with strong tip vortices and large induced velocities in the central flow region. The lift is generally well predicted but at high angles of attack (>12 deg) there is an underprediction. Separation occurs at $\alpha = 10$ deg. The drag is clearly underpredicted at high angles of attack. The significant difference between the computed drag and the experimental is a result of lift-dependent induced drag. To eliminate the lift effect on drag, the polar is shown in Fig. 10. The magnitude of the underprediction of the drag corresponds to the two-dimensional tests.

AR = 1.5

The strength of the tip vortices is reduced, and the influence of the bound vortex flow is increased. Vortex shedding of the bound vortex flow makes it impossible to find a steady-state solution above 18 deg. This angle is the stall angle predicted by Fluent. According to the experimental test,[13] stall occurs at 20 deg. The two-dimensional test already showed that the stall angle is underpredicted by Fluent by a small percentage of the angle of attack.

AR = 2

The flow is dominated by the bound vortex flow. The stall angle is reached at about 15 deg. The effect of the tip vortices is small and their influence is diffused above the stall angle because separated flow is sucked into the tip vortices. The vortices increase in size, and the pressure zone is diffused over a larger area. The incomplete reattachment of the tip vortices reduces the strength of the vortex lift and vortex drag. Although the simulations do not converge because of the bound vortex shedding, simulations at larger angle of attack show a fluctuation around $C_L = 0.65$. This plateau is also found in

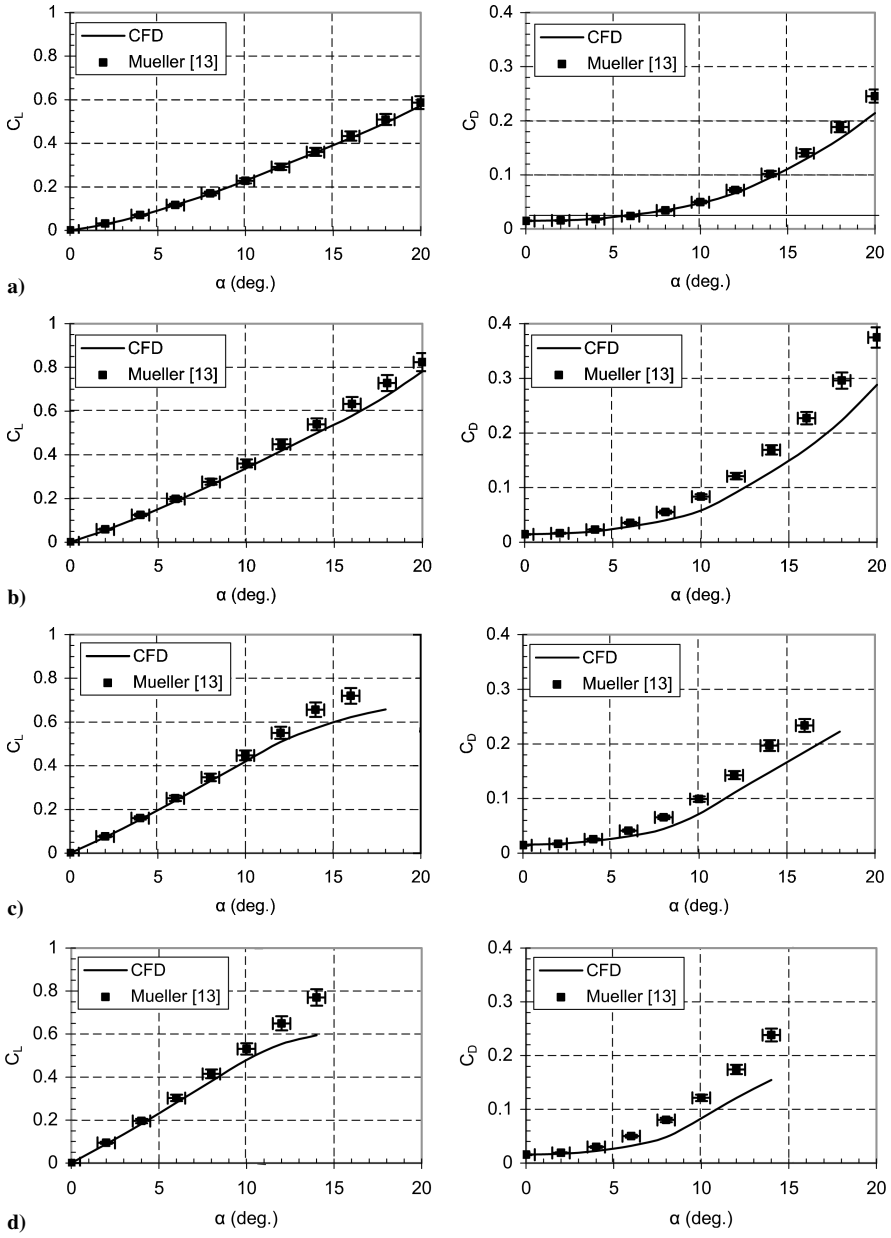

Fig. 8 C_L and C_D of flat plate; a) AR = 0.5, b) AR = 1, c) AR = 1.5, and d) AR = 2, $Re = 1 \times 10^5$.

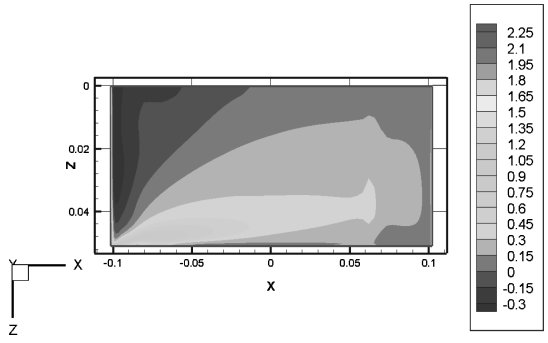

Fig. 9 Wall shear stress (m/s) of the upper surface in the X-direction, AR = 0.5, $Re = 1 \times 10^5$.

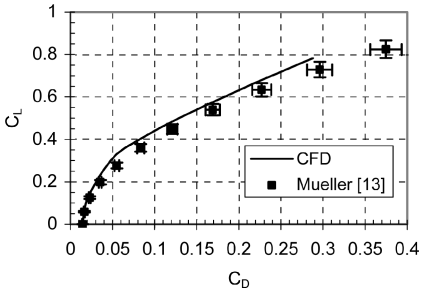

Fig. 10 Polar of flat plate, AR = 1, $Re = 1 \times 10^5$.

the experiments at a larger value, $C_L = 0.75$. This difference is again a result of the underpredicted stall angle.

3. Three-Dimensional Profiled Wing Simulations

There is no experimental data available that can be used to validate three-dimensional simulations of a profiled wing at these aspect ratios and Reynolds number. The three-dimensional simulations are compared with the flat plate simulations and the differences are discussed. This explains why the validation of the flat-plate simulation with experimental data is crucial for the investigation of a profiled wing, which is of more importance for MAVs. The results are presented in Fig. 11. To allow a good comparison, the friction drag is omitted and the zero-lift angle of attack is used. The friction drag is about 0.02 for the S5010 and 0.015 for the thinner flat plate. The difference between the geometric angle and the zero-lift angle of attack is approximately 0.7 deg for the S5010.

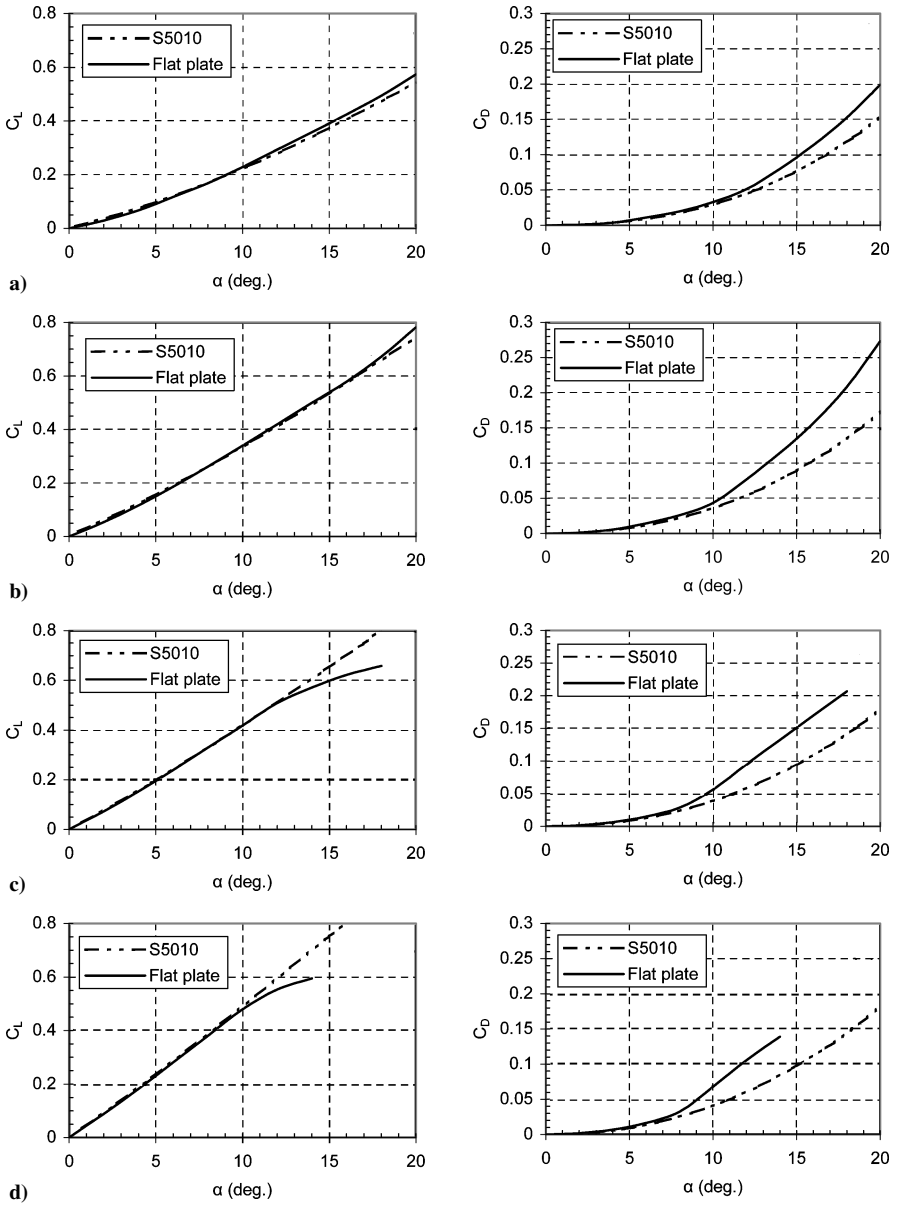

Fig. 11 Comparison of lift and profile drag of a flat plate and S5010 simulations at $Re = 1 \times 10^5$: a) AR = 0.5, b) AR = 1, c) AR = 1.5, and d) AR = 2.

For every aspect ratio, the figures show a similar result. The lift curves of the flat plate and S5010 closely match unless stall occurs, which happens earlier for the flat plate. This indicates that the vortex lift is not affected by the profile. The drag curves are similar at low angles of attack. Separation at the leading edge increases the drag of the flat plate at higher angles of attack. For $AR = 2$, the flow of the S5010 remains attached up to $C_L = 0.85$, above which a converged solution was not attainable. It is expected that the C_L value at which stall occurs will be closer to the experimental two-dimensional value, which is 1.1. At the lower-aspect-ratio range even higher values may be attainable. Torres and Mueller[13] show that rectangular flat plates with an aspect ratio of one or lower reach C_L values as high as 1.25, after which a gentle stall phenomenon occurs.

III. Strip Method

A. Limitations of the CFD Results

A comparison of the numerical simulations and experimental results of a flat plate indicated a general underprediction of the lift at large angles of attack, albeit that the differences are small. An increase in lift also leads to an increase in induced drag. At high angles of attack, at which the flow is almost completely separated, this effect is clearly visible and significant (see Fig. 8b). The difference is caused by the turbulence model. The Spalart–Allmaras model is developed for wall-bounded flows. One-equation models are often criticized for their inability to rapidly accommodate changes in length scale, such as might be necessary when the flow changes abruptly from a wall-bounded to a free shear flow. Of course, these limitations do not affect the simulations of the profiled wing, unless stall occurs. The S5010 simulations are expected to represent the experimental results in a reasonable accurate way.

The CFD simulations do not address low-Reynolds-number effects. The lack of a well-documented and validated three-dimensional transition model for wings is the main reason why such a model was not implemented. Also, the discussion later makes it clear that an implementation of such a transition model for the wings presented is not worth the effort. In reality, the flat-plate and profiled wing are subject to low-Reynolds-number effects such as separation bubbles, even at very low aspect ratios. Using a surface visualization technique, Torres and Mueller[20] discovered separations bubbles on LAR flat plates at $Re = 70000$. For the $AR = 0.5$ flat plate, a separation bubble exists near the leading edge for α between 7 and 11 deg, and for the $AR = 1$ flat plate, a separation bubble exists for α between 5 and 7 deg. The width of the separation bubble can vary from a few percent of the chord up to 20 or 30% but the spanwise zone is

limited because of the tip flow. From the experimental results of lift and drag it is clear that these effects are hardly noticeable. This is not very surprising because even a two-dimensional profile with a significant separation bubble notes a rise in profile drag in the order of 0.01. For this reason, the small separation bubble of the S5010 at α around 3 deg (two-dimensional experiments) is insignificant if compared with the total drag. The same applies to any profile with moderate low-Reynolds-number effects.

To counter the limitations of the CFD results, a numerical method was derived that uses experimental two-dimensional lift-and-drag data and a vortex lattice code to predict three-dimensional lift-and-drag data. The method is explained and validated in the next paragraph. There are actually two main reasons why this method was developed: first because of the availability of extensive databases of low-Reynolds-number profiles and second because it gives a more accurate prediction of the drag of separated flow and profiles with excessive bubble drag. These profiles are less interesting for the MAV designer but they may be useful for lower-Reynolds-number regimes (e.g., $Re < 50{,}000$), when flat plates become the best choice. The numerical simulations showed that separation is not very good simulated using a simple turbulence model such as the Spalart–Allmaras model. Detached eddy simulations could do the job, but they are still very expensive. The method discussed here, corrected for tip vortex suction effects as explained in Sec. IV, is a cheap alternative with reasonable good accuracy.

B. Method Description

The method developed is a strip method. Although the experimental data of LAR wings at low Reynolds numbers is rather limited, a lot of experimental data of two-dimensional profiles at low Reynolds numbers is available.[19] Data of many low-Reynolds-number profiles exist for different Reynolds numbers in the interesting Reynolds-number range. With the spanwise distribution of the linear lift of a wing and the experimental data of lift and drag of the profile, the strip method calculates the spanwise drag distribution of the wing excluding the vortex drag (due to the tip vortex suction).

The model developed uses an existing vortex lattice code[21] (Tornado), which uses realignment of the wake to find the distribution of the linear lift of a rectangular wing. First, the needed panel density is derived for a converged solution (200 equisized panels are sufficient, 20 spanwise and 10 chordwise). In a next step, the results of the panel method are compared with an empirical relation (Hoerner[22]) of the linear lift slope of LAR flat plates at zero angle of attack. Figure 12 gives a comparison of the slope of the lift curve $C_{L,\alpha}$ at different aspect ratios.

The strip method uses Reynolds-number-dependent experimental lift-and-drag data,[19] which are interpolated and stored in three-dimensional matrices. The wing is divided in small strips in spanwise direction (10 strips for a semispan are sufficient). The lift distribution along the span, computed by the VLM (vortex lattice method), is used as an input for the strip method. The different steps are summarized. The lift-and-drag forces are used instead of the lift-and-drag coefficients. The relationship between the three-dimensional lift L (computed by the VLM), three-dimensional drag D, local lift l, and local drag d is given in Fig. 13. The notations used for the angles are as follows: α is the angle between the wing and freestream flow, α_{2D} is the effective or local angle of attack, and ε is the downwash angle.

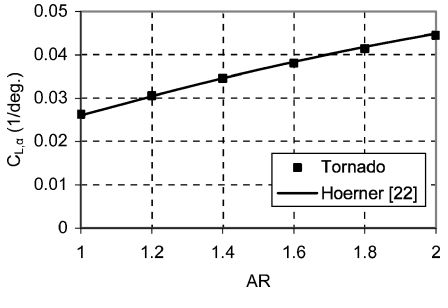

Fig. 12 Validation of the lift curve slope.

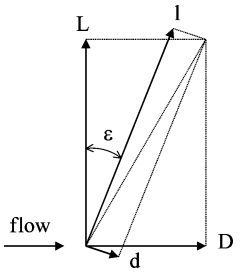

Fig. 13 Three-dimensional lift (L), three-dimensional drag (D), local lift (l), and local drag (d) of a strip.

With V_∞, α, and the three-dimensional lift (L) distribution from the VLM method, do these steps for each strip:

1) Set $\varepsilon = 0$, $d = 0$.

2) $l = (L + d \sin\varepsilon)/\cos\varepsilon$.

3) Determine local velocity $V_{2D} = V_\infty/\cos\varepsilon$ and compute local Reynolds number Re_{2D}.

4) Set l, V_{2D}, $Re_{2D} \rightarrow \alpha_{2D}$ (from experimental data using two-dimensional interpolation).

5) Let $\varepsilon = \alpha - \alpha_{2D}$.

6) Set α_{2D}, Re_{2D}, $V_{2D} \rightarrow d$ (from experimental data using two-dimensional interpolation).

7) Repeat steps 2–6 until convergence.

8) $D = d\cos\varepsilon + l\sin\varepsilon$.

The total drag of the wing is the sum over all strips of the computed spanwise three-dimensional drag (D) distribution.

This drag component is an approximation of the total drag of the wing excluding the drag due to the tip vortex suction on the wing (vortex drag). This component is added in Sec. IV. The strip method combines experimentally measured profile drag and computationally predicted induced drag. The strip method may give wrong results for flow regimes with dominant tip vortices. By adding the vortex drag to the drag predicted by the strip method, one assumes that there is no influence of the tip vortex suction on induced drag and profile drag. However, the low-pressure zones due to the tip vortex flow may eliminate the adverse pressure gradient at the tip. In this way they may suppress flow separation and low-Reynolds-number effects in this particular area. For the rectangular planform, aspect ratios, and angles of attack considered, the contribution of this area to the drag predicted by the strip method is very small.

C. Results

It is difficult to compare the results directly with experiments because the experimental results do include the suction effect of the tip vortices. However, Torres and Mueller[20] used a small angle approximation to fit the drag of a rectangular flat plate excluding vortex drag:

$$C_D = C_{D,0} + KC_L^2 \tag{1}$$

The values of K and $C_{D,0}$ are obtained by plotting C_D vs C_L^2 for three values of the Reynolds number (70,000, 100,000, 140,000) and applying a least-squares linear regression to the data. Only wind-tunnel measurements corresponding to α between –10 and 10 deg are considered to ensure linear behavior. The experiments[20] showed that the linear relation was only valid for aspect ratios of one or greater.

By applying the strip method for the α-range and the three Reynolds numbers, K and $C_{D,0}$ were predicted. The value of K is interesting because it includes a profile drag and induced drag contribution. Figure 14 shows a comparison between the predicted K and the experimental values of K (which have an uncertainty of ± 0.05 for AR = 1 and ± 0.03 for AR = 2). The strip method gives an accurate prediction.

The strip method effectively simulates the formation and disappearance of the laminar separation bubble. Starting from a zero angle of attack, the separation bubble forms when a certain effective angle is reached. For a rectangular flat plate, the spanwise downwash is the weakest at the center, which means that the critical effective angle of attack will be reached first in the center. The bubble grows in a lateral direction when the angle increases until the angle is

reached above which the flow reattaches in the center without a separation bubble (or completely detaches). Three-dimensional effects (interactions among the strips) may probably lead to more complex bubble behavior.

To account for the drag increase due to tip vortex suction, the drag predicted by the strip method is added to the vortex drag predicted by an existing formula. This is explained in Sec. IV.

IV. Lift and Drag Equations

The models of the vortex lift and drag are based on the leading-edge suction analogy, which was first introduced by Polhamus[10] for lift prediction of thin delta wings and extended by Lamar[11,23] for rectangular planforms and planforms with longitudinal side edges. The suction analogy states that the extranormal force that is produced by a highly swept wing or LAR wing at high angles of attack is equal to the loss of leading-edge and side-edge suction associated with the separated flow. The analogy leads to the following relationship for the additional normal-force coefficient:

$$C_{N,v} = K_{v,le}|\sin\alpha|\sin\alpha + K_{v,se}|\sin\alpha|\sin\alpha = K_v|\sin\alpha|\sin\alpha \tag{2}$$

A projection of the normal force coefficient along the free-flow axis and the axis normal to the free flow gives the vortex drag and vortex lift:

$$C_{L,v} = K_v|\sin\alpha|\sin\alpha\cos\alpha \tag{3}$$

$$C_{D,v} = K_v\sin^3\alpha \tag{4}$$

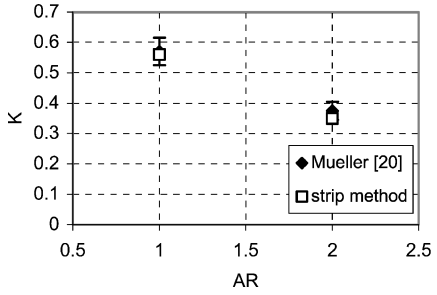

Fig. 14 Comparison of K derived by experimental data and the strip method.

The vortex lift factor, K_v, is the sum of the leading-edge vortex lift factor and side-edge vortex lift factor. Lamar used a modified lifting-surface theory to estimate the relative contributions to the lift force of the leading edge and side edges. For LAR rectangular planforms and generally for most LAR planforms (cropped delta wings, Zimmerman, elliptical planforms, etc.) in the aspect-ratio range 0.5–1.5, the vortex lift factor is close to π, as long as the tip vortex systems remains attached. For a rectangular planform and an AR of 1, the values are $K_{v,le} = 0.782$ and $K_{v,se} = 2.126$ (Ref. 24). Using these equations and the potential lift, Polhamus[10] found an equation for C_L and Lamar[23] proposed an equation for C_D:

$$C_L = C_{L,p} + C_{L,v} = K_p\sin\alpha\cos^2\alpha + K_v|\sin\alpha|\sin\alpha\cos\alpha \tag{5}$$

$$C_D = C_{D,0} + C_L|\tan\alpha| = C_{D,0} + K_p|\sin\alpha|\sin\alpha\cos\alpha + K_v\sin^3\alpha \tag{6}$$

The lift equation is in very good agreement with CFD results and experiments (see Fig. 15 for profiled wings and Fig. 16 for flat plates). According to Polhamus (cited by Lamar and Campbell[24]), the normal force is reduced in the case of a rounded leading edge, as some of it remains as "residual" leading-edge suction in the wing plane, but the sum of the residual leading-edge suction and normal force adds up to the total leading-edge suction available. This explains the fact that Eq. (5) is still valid for wings with profiles or rounded leading edges. The drag equation has its limitations. The proposed drag equation of Lamar is only applicable to a wing without leading-edge suction. This happens when the flow at the leading edge is separated and the aerodynamic force is normal to the wing. A very thin flat plate is an example of such a wing. Thicker plates with a rounded leading edge, such as those used by Mueller, have leading-edge suction in the lower alpha range and no leading-edge suction in the higher alpha range. This is probably one of the reasons why Mueller found that the Lamar equation for the drag did not fit well with the experimental data. Profiled wings, such as the S5010, have leading-edge suction in the prestall region unless a laminar separation bubble is formed, which will reduce the leading-edge suction effect (and hence increase the drag).

The present research proposes two solutions to this problem: a general solution based on the strip method and a formula for profiled wings based on the flow physics. The latter formula can be derived if we split the drag in its basic components: a friction drag term, a term associated with the bounded vortex (induced drag), and a term associated with the tip vortices (vortex drag). If we consider

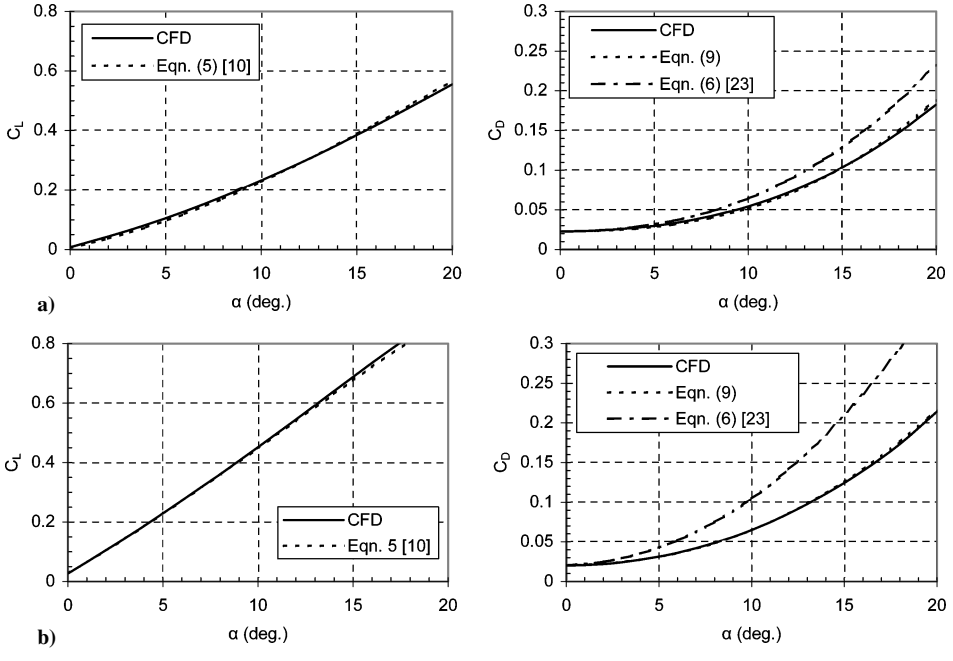

Fig. 15 Comparison of CFD lift (S5010) with Eq. (5) and CFD drag (S5010) with Eqs. (6) and (9), a) AR = 0.5 and b) AR = 1.5, $Re = 1 \times 10^5$.

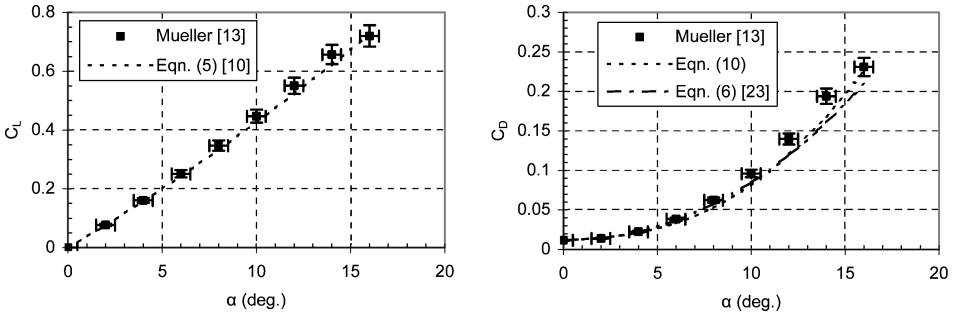

Fig. 16 Comparison of lift and drag of experiments (flat plate) with Eqs. (5) and (10), respectively, AR = 1.5, $Re = 1 \times 10^5$.

an average downwash angle ε, the formula becomes

$$C_D = C_{D,0} + C_{L,p}|\tan\varepsilon| + C_{D,v} \tag{7}$$

A lifting line approximation of ε is well known:

$$\tan\varepsilon = (K_p/e\pi AR)\sin\alpha \tag{8}$$

where e is the Oswald or efficiency factor. Hoerner[25] showed that this relationship also holds for LAR wings. The value of $e \approx 1$ for wings with flat or sharp lateral edges, and $e \approx 0.85$ for wings with rounded lateral edges. Using this relation and the equation of the vortex drag, the formula of the drag coefficient for profiled LAR wings becomes

$$C_D = C_{D,0} + \left(K_p^2/e\pi AR\right)|\sin\alpha|\sin\alpha\cos^2\alpha + K_v\sin^3\alpha \tag{9}$$

K_p may be derived using a VLM method, a surface-integral method, or empirical approximations (Hoerner[22]), which all closely agree. K_v may be derived using the method of Lamar. Based on this method, a good approximation for K_v is 2.9 for AR < 1.5. For rectangular wings at larger AR values, the leading-edge vortex seems to detach and only the side-edge vortex remains. This is in agreement with the experiments of Torres and Mueller,[13] who discovered that separation of the tip vortex system occurs at much lower angles above an aspect ratio of 1.5. According to Lamar, a good approximation for AR ≥ 1.5 is 2.1. When we used these approximations, a very good agreement between Eq. (9) and the CFD results was found. Figure 15 shows the results for AR = 0.5 and AR = 1.5. The figure also shows Eq. (6), which clearly overpredicts the drag.

A second solution includes the strip method. It is a more general method, which is also applicable for flat plates or wings exhibiting large laminar separation regions. The equation for the total lift is still Eq. (5) with K_p predicted by the VLM method. The total drag is now

$$C_D = C_{D,\text{strip}} + K_v\sin^3\alpha \tag{10}$$

Figure 16 shows the results for the flat plate ($AR = 1.5$, $K_v = 2.1$) and compares it with the experiments of Torres and Mueller.[13] In general there is a good agreement, but the experiments of Mueller still show a somewhat higher drag at high angles of attack. Equation (6) also predicts the drag reasonable well.

V. Conclusion

The aerodynamic forces acting on LAR wings are studied using CFD simulations, a strip method, and experimental data. The study is focused on wings with an aspect ratio between 0.5 and 2 at a representative Reynolds number of 100,000. These wings are of primary interest for MAV applications, whose development is hindered by a lack of accurate models that can predict the primary aerodynamic forces for performance- and dynamics-related optimization studies. Two different wing types are studied: a flat-plate wing, representative for a wing–tail–fuselage type of MAV, and a profiled wing (S5010), representative for a flying-wing MAV.

A total of 88 CFD simulations were performed to find the lift-and-drag curves of the flat plate and the profiled wing at four different aspect ratios and angles of attack up to 20 deg. The Spalart–Allmaras turbulence model was used because it turned out to be the most accurate model available. The primary purpose of the simulations was the study of the nonlinearities in lift and, especially, the drag. The flat-plate simulations were compared with experimental data, and in general there was a very good agreement between simulations and experiments. An underprediction of the lift and the drag was visible at flow conditions dominated by separation. The difference was attributed to the turbulence model. A comparison of the flat-plate simulations and the profiled-wing simulations showed no significant difference in the lift curve. The vortex normal force is not affected by the profile. The drag curves are similar as long as the flat plate exhibits a leading-edge suction effect. Leading-edge separation leads to an increase in flat-plate drag. There are no three-dimensional experiments available for the S5010 wing but the lack of separated flow indicates that the CFD results may closely agree with the experiments. The lift of the S5010 and flat plate are almost identical but the drag level of the S5010 is clearly lower because of leading-edge suction.

A strip method was developed to include low-Reynolds-number effects, such as laminar separation bubbles, and to give a better prediction of drag due to separation. The method uses experimental lift-and-drag data of the two-dimensional profile and a vortex lattice code to predict three-dimensional lift-and-drag data. It does not include vortex lift and drag. Comparison with experimental data at low angles of attack showed its success.

Finally, two formalized methods to predict the drag of LAR wings were described. The lift was found to be accurately described by an existing analytically derived formula. Of primary importance was an accurate formulation for the tip vortices, which was found using a technique of Lamar. A method to predict the drag was derived from existing analytical models. It is applicable to profiled wings with moderate low-Reynolds-number effects. The results are in very good agreement with the CFD simulations of the profiled wing. It could be a cheap alternative to CFD for MAV optimization studies. The second method includes the strip method and is generally applicable. It needs experimental two-dimensional data of the wing profile. It is in good agreement with the experimental results.

Acknowledgments

The research is supported by the Special Research Fund of Ghent University (BOF2002/DRMAN/052).

References

[1]McMichael, J., "Micro Air Vehicles," DARPA briefing at the DUSD (S&T) Seminar on Emerging Technologies: Micro Air Vehicles, Alexandria, VA, Dec. 11, 1998.

[2]Grasmeyer, J. M., and Keennon, M. T., AeroVironment, "Development of the Black Widow Micro Air Vehicle," AIAA Paper 2001-0127, Jan. 2001.

[3]Kellogg, J., Bovais, G., Dahlburg, J., Foch, R., Gardner, J., Gordan, D., Hartley, R., Kamgar-Parsi, B., McFarlane, H., Pipitone, F., Ramamurthi, R., Sciambi, A., Spears, W., Srull, D., and Sullivan, C., "The NRL Mite Air Vehicle," *Proceedings of the 16th International Conference on Unmanned Air Vehicle Systems*, Univ. of Bristol, Bristol, England, U.K., 2001, pp. 25-1–25-14.

[4]Peterson, B., Erath, B., Henry, K., Lyon, M., Walker, B., Powell, N., Fowkes, K., and Bowman, W. J., "Development of a Micro Air Vehicle for Maximum Endurance and Minimum Size," AIAA Paper 2003-416, Jan. 2003.

[5]Ifju, P. G., Jenkins, D. A., Ettinger, S., Lian, Y., Shyy, W., and Waszak, M. R., "Flexible-Wing-Based Micro Air Vehicles," AIAA Paper 2002-705, Jan. 2002.

[6]Shyy, W., Berg, M., and Ljungqvist, D., "Flapping and Flexible Wings for Biological and Micro Air Vehicles," *Progress in Aerospace Sciences*, Vol. 35, July 1999, pp. 455–505.

[7]Michelson, R. C., and Naqvi, M. A., "Beyond Biologically-Inspired Insect Flight," RTO/AVT VKI Lecture Series on "Low Reynolds Number Aerodynamics on Aircraft Including Applications in Emerging UAV Technology," VKI, Rhode-Saint-Genèse, Belgium, Nov. 2003.

[8]Bohorquez, F., Rankins, F., and Baeder, J, "Hover Performance of Rotor Blades at Low Reynolds Numbers for Rotary Wing Micro Air Vehicles: An Experimental and CFD Study," AIAA Paper 2003-3930, June 2003.

[9]Bollay, W., "A Non-Linear Wing Theory and Its Application to Rectangular Wings of Small Aspect Ratio," *Zeitschrift Fur Angewandte Mathematik und Mechanik*, Vol. 19, 1939, pp. 21–35.

[10]Polhamus, E. C., "Predictions of Vortex-Lift Characteristics by a Leading-Edge-Suction Analogy," *Journal of Aircraft*, Vol. 8, No. 4, 1971, pp. 193–199.

[11]Lamar, J. E., "Extension of Leading-Edge-Suction Analogy to Wings with Separated Flow Around the Side Edges at Subsonic Speeds," NASA TR R-428, L-9460, Oct. 1974.

[12]Mueller, T. J., "Aerodynamic Measurements at Low Reynolds Numbers for Fixed Wing Micro Aerial Vehicles," RTO AVT/VKI Special Course on Development and Operation of UAVs for Military and Civil Applications, VKI, Rhode-Saint-Genèse, Belgium, Sept. 1999.

[13]Torres, G. E., and Mueller, T. J., "Low-Aspect-Ratio Wing Aerodynamics at Low Reynolds Numbers," *AIAA Journal*, Vol. 42, No. 5, 2004, pp. 865–873.

[14]Winter, H., "Flow Phenomena on Plates and Airfoils of Short Span," NACA TM 798, July 1936.

[15]Reynolds, W. C., and Carr, L. W., "Review of Unsteady, Driven, Separated Flows," AIAA Paper 85-0527, March 1985.

[16]Elle, B. J., "An Investigation at Low Speed of the Flow near the Apex of Thin Delta Wings with Sharp Leading Edges," Aeronautical Research Council, R&M3176 ARC-19780, His Majesty's Stationary Office, London, 1961.

[17]Erickson, G. E., "Water-Tunnel Studies of Leading-Edge Vortices," *Journal of Aircraft*, Vol. 21, No. 5, 1984, pp. 442–448.

[18]Spalart, P. R., and Allmaras, S. R., "A One-Equation Turbulence Model for Aerodynamic Flows," *La Recherche Aerospatiale*, Vol. 1, No. 1, 1994, pp. 5–21.

[19]Selig, M. S., Lyon, C. A., Giguère, P., Ninham, C. P., and Guglielmo, J. J., *Summary of Low-Speed Airfoil Data,* Vol. 2, Soartech Publications, Virginia Beach, VA, pp. 142–145.

[20]Torres, G. E., and Mueller, T. J., "Aerodynamic Characteristics of Low Aspect Ratio Wings at Low Reynolds Numbers," *Fixed and Flapping Wing Aerodynamics for Micro Air Vehicle Applications*, edited by T. J. Mueller, Progress in Astronautics and Aeronautics, Vol. 195, AIAA, Reston, VA, 2001, pp. 115–141.

[21]Melin, T., *A Vortex Lattice MATLAB Implementation for Linear Aerodynamic Wing Applications*, TORNADO Release 1.23b, URL: http://www.ave.kth.se/divisions/aero/software/tornado [cited 9 April 2003].

[22]Hoerner, S. F., and Borst, H. V., *Fluid-Dynamic Lift*, Hoerner Fluid Dynamics, Brick Town, NJ, 1975, pp. 17–3.

[23]Lamar, J. E., "Prediction of Vortex Flow Characteristics of Wings at Subsonic and Supersonic Speeds," *Journal of Aircraft*, Vol. 13, No. 7, 1976, pp. 490–494.

[24]Lamar, J. E., and Campbell, J. F., "Recent Studies at NASA Langley of Vortical Flows Interacting with Neighboring Surfaces," *Aerodynamics of Vortical Type Flows in Three Dimensions*, AGARD CP No. 342, Neuilly sur Seine, France, 1983.

[25]Hoerner, S. F., *Fluid-Dynamic Drag*, Hoerner Fluid Dynamics, Brick Town, NJ, 1965, Chap. 7, pp. 7–17.